AIAA Paper 2008-0745

Calculation of Transonic Flows Using WENO Method with a Low Diffusion E-CUSP Upwind Scheme

Ge-Cheng Zha* Yiqing Shen † Baoyuan Wang ‡
Dept. of Mechanical and Aerospace Engineering
University of Miami
Coral Gables, Florida 33124
E-mail: gzha@miami.edu

Abstract

A low diffusion E-CUSP (LDE) scheme is applied with 5th order WENO scheme in this paper. The E-CUSP scheme can capture crisp shock profile and exact contact surface. Several numerical cases are presented to demonstrate the accuracy and robustness for the E-CUSP scheme to be used with the WENO strategy.

1 Introduction

With the application of computational fluid dynamics becoming more and more popular, the demand on high accuracy and high efficiency CFD solutions also becomes stronger to satisfy the needs of the broad engineering problems. So far, most of the engineering applications employ the 2nd order numerical accuracy. The high order schemes (higher than 3rd order) are mostly limited to the fundamental research such as high fidelity turbulence simulation (e.g. Large Eddy Simulations and Direct Numerical Simulation) and aeroacoustics calculation. The reason is that the high order schemes are generally not mature enough for robust engineering applications.

For aerospace engineering applications with shock waves or contact surfaces, the essentially non-oscillatory (ENO) or weighted essentially non-oscillatory (WENO) schemes are attractive for their capability to treat the discontinuities and achieve the consistent high order accuracy in the smooth regions. By using a convex combination of all candidate stencils to replace the smoothest one in ENO scheme, the WENO scheme has more advantages over its base ENO scheme, for example, it approaches high order optimal accuracy in smooth regions, has better convergence rate due to the smooth numerical flux is used. From its presence [1, 2] to present, the WENO schemes have been extensively developed and applied to different flow problems.

To achieve the purpose of efficiency, accuracy and easiness to use, many efforts have been made to develop upwind schemes only using scalar dissipation instead of matrix dissipation such as that of the Roe's flux difference splitting (FDS) scheme [3]. The examples include AUSM family schemes of Liou

* Associate Professor, AIAA Senior Member
† Research Scientist, AIAA Member
‡ Ph.D. Candidate

[4, 5, 6, 7, 8], the Van Leer-Hänel scheme[9], Edwards's LDFSS schemes[10, 11], Jameson's CUSP schemes and limiters[12, 13, 14], and the E-CUSP schemes developed by Zha, et al.[15, 16, 17, 18], etc.

Pioneered by Liou and Steffen[4, 6, 7], the researchers seeking the scalar dissipation primarily follow the guideline that the velocity and pressure should be separated to consider their characteristics representing the physics of the convection and waves. Liou and his colleagues termed their schemes as advection upstream splitting method(AUSM) schemes, and Jameson gave the name of convective upwind and split pressure (CUSP) schemes[12, 13, 14].

The CUSP schemes can be basically categorized to two types, the H-CUSP and E-CUSP[12, 13, 14]. The H-CUSP schemes have the total enthalpy from the energy equation in their convective vector, while the E-CUSP schemes use the total energy in the convective vector. The Liou's AUSM family schemes, Van Leer-Hänel scheme[9], and Edwards's LDFSS schemes[10, 11] belong to the H-CUSP group. The schemes developed by Zha, et al.[15, 16, 17, 18] belong to the E-CUSP group.

Even though the H-CUSP schemes such as AUSM family schemes have achieved great success, from the characteristic theory point of view, the schemes are not fully consistent with the disturbance propagation directions[19, 20], which may affect the stability and robustness of the schemes. By splitting the eigenvalues of the Jacobians to convection (velocity) and waves (speed of sound), one will find that the convection terms only contain the total energy[15], which will lead to the E-CUSP schemes.

Zha and Hu recently suggested an E-CUSP schemes, which has low diffusion and can capture crisp shock wave profiles and exact contact discontinuities[18]. The scheme is consistent with the characteristic directions due to the nature of E-CUSP scheme. The scheme shows the highest stability for two shock tube tests problems compared with several other popularly used upwind schemes for the explicit Euler time marching scheme. The scheme also works well when extended to multi-dimensions[18]. However, the E-CUSP scheme of Zha-Hu may generate temperature oscillation near the computation boundary, in particular when the mesh is skewed. Zha was able to remove the temperature oscillation by introducing the total enthalpy in the smooth factor for the energy equation[19, 20]. However, the scheme loses the capability to capture the exact contact surface due to the modification.

The purpose of this paper is to apply an improved low diffusion and efficient E-CUSP upwind scheme with the WENO scheme to capture the discontinuities and achieve high order accuracy in the smooth regions. This paper proposes a modification of the Zha-Hu E-CUSP scheme by using the Mach number splitting of Edwards's LDFSS schemes[10] for the convective flux. The solutions calculated by the new scheme is smooth and the scheme can capture crisp shock profile and exact contact discontinuity. The scheme is shown to be accurate, robust and efficient by the cases tested in this paper with and without WENO scheme.

2 The Numerical Scheme

2.1 Governing Equations

To describe the new scheme, we will begin with the quasi-1D Euler equations in Cartesian coordinates for inviscid flow:

$$\partial_t \mathbf{U} + \partial_x \mathbf{E} - \mathbf{H} = 0 \tag{1}$$

where $\mathbf{U} = S\mathbf{Q}$, $\mathbf{Q} = \begin{pmatrix} \rho \\ \rho u \\ \rho e \end{pmatrix}$, $\mathbf{E} = S\mathbf{F}$,

$$\mathbf{F} = \begin{pmatrix} \rho u \\ \rho u^2 + p \\ (\rho e + p)u \end{pmatrix}, \quad \mathbf{H} = \frac{dS}{dx} \begin{pmatrix} 0 \\ p \\ 0 \end{pmatrix} \tag{2}$$

In above equations, ρ is the density, u is the velocity, p is the static pressure, e is the total energy per unit mass and S is the cross sectional area of the 1D duct. The following state equation is also employed:

$$p = (\gamma - 1)(\rho e - \frac{1}{2}\rho u^2) \tag{3}$$

where γ is the specific heat ratio with the value of 1.4 for ideal gas.

The finite volume method with the explicit Euler temporal integration is used to discretize the governing equations. It yields the following formulation at cell i:

$$\Delta \mathbf{Q}_i^{n+1} = \Delta t[-C(\mathbf{E}_{i+\frac{1}{2}} - \mathbf{E}_{i-\frac{1}{2}}) + \frac{\mathbf{H}_i}{S_i}]^n \tag{4}$$

where $C = 1/(\Delta x S_i)$, n is the time level index. A numerical scheme is needed to evaluate the interface flux:

$$\mathbf{E}_{i+\frac{1}{2}} = S\mathbf{F}_{i+\frac{1}{2}} \tag{5}$$

2.2 The Low Diffusion E-CUSP Scheme

In [15, 16, 18], the characteristic analysis is given as the foundation to construct the E-CUSP scheme. The basic idea is to split the flux $\mathbf{F}$ to the convective flux $\mathbf{F^c}$ and the pressure flux $\mathbf{F^p}$. That is:

$$\mathbf{F} = \mathbf{F^c} + \mathbf{F^p} = \begin{pmatrix} \rho u \\ \rho u^2 \\ \rho e u \end{pmatrix} + \begin{pmatrix} 0 \\ p \\ p u \end{pmatrix} \tag{6}$$

The vector $\mathbf{F^c}$ has the eigenvalues of the velocity (u, u, u), which represent the convective terms. The vector $\mathbf{F^p}$ has the eigenvalues of the speed of sound, $(-a, 0, a)$, which represents the acoustic waves propagating in each direction at subsonic regime.

Based on the above separation of convective and wave terms in subsonic regime, Zha et al.[15, 16, 17, 18] suggested to treat the convective term $\mathbf{F^c}$ in an upwind manner and to average the wave term $\mathbf{F^p}$ in both upwind and downwind direction with the weight of $u \pm a$. Such a construction of the upwind scheme is consistent with the characteristic directions.

In this paper, the modified E-CUSP scheme will have the same pressure splitting as that in [18, 20]. The convective flux will be based on the Mach number splitting instead of the mass flux splitting. It can be written as:

$$\mathbf{F^c} = u \begin{pmatrix} \rho \\ \rho u \\ \rho e \end{pmatrix} = aM\mathbf{f^c} \tag{7}$$

where, a is the speed of sound, M is the Mach number, and

$$\mathbf{f^c} = \begin{pmatrix} \rho \\ \rho u \\ \rho e \end{pmatrix} \tag{8}$$

Similar to the treatment in [7, 16, 10], the interface speed of sound will be used in order to capture the contact discontinuities. The present E-CUSP scheme will adopt the Mach number splitting of Edwards [10], which is derived from the van Leer's Mach number splitting formulation [21] and is made to capture the contact discontinuities.

The interface flux of the present E-CUSP scheme is given as the following in the subsonic regime:

$$\mathbf{F}_{\frac{1}{2}} = a_{\frac{1}{2}}(C^+(M)\mathbf{f^c}_L + C^-(M)\mathbf{f^c}_R) + \begin{pmatrix} 0 \\ \mathcal{P}^+ p \\ \frac{1}{2}p(u + a_{\frac{1}{2}}) \end{pmatrix}_L + \begin{pmatrix} 0 \\ \mathcal{P}^- p \\ \frac{1}{2}p(u - a_{\frac{1}{2}}) \end{pmatrix}_R \tag{9}$$

The interface speed of sound $a_{\frac{1}{2}}$, Mach number, u_L^+, and u_R^+ are evaluated as:

$$a_{\frac{1}{2}} = \frac{1}{2}(a_L + a_R) \tag{10}$$

$$M_L = \frac{u_L}{a_{\frac{1}{2}}}, \qquad M_R = \frac{u_R}{a_{\frac{1}{2}}} \tag{11}$$

In subsonic regime, if the flow is in the the direction, $0 \leq u \leq a$,

$$C^+(M) = \frac{1}{4}(M_L + 1)^2 - \frac{1}{4}(M_L - 1)^2\epsilon_1 \tag{12}$$

$$C^-(M) = -\frac{1}{4}(M_R - 1)^2 + \frac{1}{4}(M_L - 1)^2\epsilon_2 \tag{13}$$

It can be seen, if $\epsilon_1 = \epsilon_2 = 1$, the Mach number splitting is the Van Leer's Mach number splitting [21]. The ϵ_1 and ϵ_2 are evaluated as[10]:

$$\epsilon_1 = \frac{a_R + a_L\phi}{a_R + a_L} \tag{14}$$

$$\epsilon_2 = \frac{a_L + a_R/\phi}{a_R + a_L} \tag{15}$$

where,

$$\phi = \frac{(\rho a^2)_R}{(\rho a^2)_L} \tag{16}$$

For most of the cases, ϵ_1 and ϵ_2 are on the order of 1 except at the shock discontinuities. The convective flux is hence primarily evaluated by the upwind flux.

In subsonic regime, if the flow is in the direction, $-a \leq u \leq 0$, the Mach number splitting is constructed following the symmetric rule, which is:

$$C^+(M) = \frac{1}{4}(M_L + 1)^2 - \frac{1}{4}(M_R + 1)^2\epsilon_1 \tag{17}$$

$$C^-(M) = -\frac{1}{4}(M_R - 1)^2 + \frac{1}{4}(M_R + 1)^2\epsilon_2 \tag{18}$$

The pressure splitting coefficient borrowed from Van Leer[21] is used:

$$\mathcal{P}^{\pm}_{L,R} = \frac{1}{4}(M_{L,R} \pm 1)^2(2 \mp M_{L,R}) \tag{19}$$

For supersonic flows,

If $u > a$, $\mathbf{F}_{\frac{1}{2}} = \mathbf{F}_L$; If $u < -a$, $\mathbf{F}_{\frac{1}{2}} = \mathbf{F}_R$

Above formulations can be written as a general form considering the Mach number range $-\infty < M < \infty$, which is given in the following section describing the extension of the scheme to 3D.

2.3 Extension to Multi-Dimensions

2.3.1 Governing Equations

The normalized Navier-Stokes equations governing compressible viscous flows in three-dimensions can be written in the Cartesian coordinate as:

$$\frac{\partial Q}{\partial t} + \frac{\partial E}{\partial x} + \frac{\partial F}{\partial y} + \frac{\partial G}{\partial z} = \frac{1}{Re}\left(\frac{\partial R}{\partial x} + \frac{\partial S}{\partial y} + \frac{\partial T}{\partial z}\right) \tag{20}$$

where

$$Q = \begin{bmatrix} \rho \\ \rho u \\ \rho v \\ \rho w \\ \rho e \end{bmatrix}, E = \begin{bmatrix} \rho u \\ \rho u^2 + p \\ \rho uv \\ \rho uw \\ (\rho e + p)u \end{bmatrix}, F = \begin{bmatrix} \rho v \\ \rho uv \\ \rho v^2 + p \\ \rho vw \\ (\rho e + p)v \end{bmatrix}, G = \begin{bmatrix} \rho w \\ \rho uw \\ \rho vw \\ \rho w^2 + p \\ (\rho e + p)w \end{bmatrix},$$

$$R = \begin{bmatrix} 0 \\ \tau_{xx} \\ \tau_{xy} \\ \tau_{xz} \\ u_k\tau_{xk} - q_x \end{bmatrix}, S = \begin{bmatrix} 0 \\ \tau_{xy} \\ \tau_{yy} \\ \tau_{yz} \\ u_k\tau_{yk} - q_y \end{bmatrix}, T = \begin{bmatrix} 0 \\ \tau_{xz} \\ \tau_{yz} \\ \tau_{zz} \\ u_k\tau_{zk} - q_z \end{bmatrix},$$

The repeated index k stands for the Einstein summation over x, y and z. The stress τ and heat flux q are,

$$\tau_{ik} = (\mu + \mu_t)\left[(\frac{\partial u_i}{\partial x_k} + \frac{\partial u_k}{\partial x_i}) - \frac{2}{3}\delta_{ik}\frac{\partial u_j}{\partial x_j}\right]$$

$$q_j = \frac{-1}{(\gamma - 1)M^2_\infty}(\frac{\mu}{Pr} + \frac{\mu_t}{Pr_t})\frac{\partial T}{\partial x_j}$$

The equation of state is

$$\rho e = \frac{p}{\gamma - 1} + \frac{1}{2}\rho(u^2 + v^2 + w^2)$$

where μ_t is the turbulence eddy viscosity calculated by Baldwin-Lomax(BL) model[22].

In the above equations, ρ is the density, u, v, and w are the Cartesian velocity components in x, y and z directions, p is the static pressure, and e is the total energy per unit mass, μ is the molecular viscosity, J is the transformation Jacobian, γ, Re, M_∞, Pr *and* Pr_t are the ratio of specific heat, Reynolds number, freestream Mach number, Prandtl number and turbulent Prandtl number, respectively.

2.4 The LDE Scheme in 3-Dimensions[23]

The extension of the LED scheme to 3D is straightforward and is basically the same as the 1D scheme. In generalized coordinate system, the flux **E** can be split as the following

$$\mathbf{E} = E^c + E^p = \begin{pmatrix} \rho U \\ \rho u U \\ \rho v U \\ \rho w U \\ \rho e U \end{pmatrix} + \begin{pmatrix} 0 \\ l_x p \\ l_y p \\ l_z p \\ p\overline{U} \end{pmatrix} \tag{21}$$

where, U is the contravariant velocities in ξ direction expressed as

$$U = l_t + l_x u + l_y v + l_z w \tag{22}$$

where, $\mathbf{l}$ is the normal vector on ξ surfaces with its magnitude equal to the elemental surface area and pointing to the direction of increasing ξ.

$$\mathbf{l} = \frac{\nabla \xi}{J} \mathrm{d}\eta \mathrm{d}\zeta \tag{23}$$

l_t stands for the grid moving velocity and is defined as

$$l_t = \frac{\xi_t}{J} \mathrm{d}\eta \mathrm{d}\zeta \tag{24}$$

The velocity $\overline{U}$ is defined as

$$\overline{U} = U - l_t = l_x u + l_y v + l_z w \tag{25}$$

In multi-dimensions, the formulations given in section 2.2 can be written in a general form from subsonic to supersonic with $-\infty < M < \infty$ as the following.

The convective term, E^c is evaluated as,

$$E^c = \rho U \begin{pmatrix} 1 \\ u \\ v \\ w \\ e \end{pmatrix} = \rho U f^c, \; f^c = \begin{pmatrix} 1 \\ u \\ v \\ w \\ e \end{pmatrix} \tag{26}$$

let

$$C = c \left(l_x^2 + l_y^2 + l_z^2 \right)^{\frac{1}{2}} \tag{27}$$

where $c = \sqrt{\gamma RT}$ is the speed of sound. Then the convective flux at interface $\frac{1}{2}$ is evaluated as:

$$E^c_{\frac{1}{2}} = C_{\frac{1}{2}} \left[\rho_L C^+ f^c_L + \rho_R C^- f^c_R \right] \tag{28}$$

where, the subscripts L and R represent the left and right hand sides of the interface. The interface speed of sound is

$$C_{\frac{1}{2}} = \frac{1}{2} \left(C_L + C_R \right) \tag{29}$$

The following relations borrowed from Edwards LDFFS scheme [10, 11] to express the formulations from $-\infty < M < \infty$ are used,

$$\begin{array}{l}
C^+ = \alpha^+_L \left(1 + \beta_L\right) M_L - \beta_L M^+_L - M^+_{\frac{1}{2}} \\
C^- = \alpha^-_R \left(1 + \beta_R\right) M_R - \beta_R M^-_R + M^-_{\frac{1}{2}} \\
M_L = \frac{U_L}{C_{\frac{1}{2}}},\ M_R = \frac{U_R}{C_{\frac{1}{2}}} \\
\alpha_{L,R} = \frac{1}{2} \left[1 \pm sign \left(M_{L,R} \right) \right] \\
\beta_{L,R} = -max \left[0, 1 - int \left(|M_{L,R}| \right) \right] \\
M^+_{\frac{1}{2}} = M_{\frac{1}{2}} \frac{C_R + C_L \Phi}{C_R + C_L},\ M^-_{\frac{1}{2}} = M_{\frac{1}{2}} \frac{C_L + C_R \Phi^{-1}}{C_R + C_L},\ \Phi = \frac{\left(\rho C^2\right)_R}{\left(\rho C^2\right)_L} \\
M_{\frac{1}{2}} = \beta_L \delta^+ M^-_L - \beta_R \delta^- M^+_R \\
M^\pm_{L,R} = \pm \frac{1}{4} \left(M_{L,R} \pm 1 \right)^2 \\
\delta^\pm = \frac{1}{2} \left\{ 1 \pm sign \left[\frac{1}{2} \left(M_L + M_R \right) \right] \right\}
\end{array} \tag{30}$$

The pressure flux, E^p is evaluated as the following

$$E^p_{\frac{1}{2}} = \begin{pmatrix} 0 \\ p\, l_x \\ p\, l_y \\ p\, l_z \\ p\overline{U} \end{pmatrix} = \begin{pmatrix} 0 \\ \left(\mathcal{D}^+_L p_L + \mathcal{D}^-_R p_R \right) l_x \\ \left(\mathcal{D}^+_L p_L + \mathcal{D}^-_R p_R \right) l_y \\ \left(\mathcal{D}^+_L p_L + \mathcal{D}^-_R p_R \right) l_z \\ \overline{C}_{\frac{1}{2}} \left(\mathcal{S}^+_L p_L + \mathcal{S}^-_R p_R \right) \end{pmatrix} \tag{31}$$

where,

$$\mathcal{D}^\pm{}_{L,R} = \left[\alpha \left(1 + \beta \right) - \beta \mathcal{P}^\pm \right]_{L,R} \tag{32}$$

The pressure splitting coefficient is:

$$\mathcal{P}^\pm_{L,R} = \frac{1}{4} \left(M_{L,R} \pm 1 \right)^2 \left(2 \mp M_{L,R} \right) \tag{33}$$

For the pressure term in the energy equation, the contravariant speed of sound $\overline{C}$ is consistent with $\overline{U}$ and is calculated as:

$$\overline{C} = C - l_t \tag{34}$$

$$\mathcal{S}^\pm{}_{L,R} = \left[\bar{\alpha}^\pm \left(1 + \bar{\beta} \right) M - \bar{\beta} \bar{M} \right]_{L,R} \tag{35}$$

where

$$\bar{M} = \frac{\overline{U}}{\overline{C}} \tag{36}$$

and the $\bar{\alpha}$ and $\bar{\beta}$ are evaluated based on $\bar{M}$ using the formulations given in eq. (30). The use of $\overline{U}$, $\overline{C}$ and $\bar{M}$ in the pressure term for the energy equation is to take into account of the grid speed so that the flux will transit from subsonic to supersonic smoothly. When the grid is stationary, $l_t = 0$, $\overline{C} = C$, $\overline{U} = U$.

2.5 The WENO Scheme[24]

The fifth-order accurate WENO ($r = 3$) reconstruction of u^L and u^R can be written as

$$u^L_{i+1/2} = \omega_0 q_0 + \omega_1 q_1 + \omega_2 q_2$$

where

$$q_0 = \frac{1}{3}u_{i-2} - \frac{7}{6}u_{i-1} + \frac{11}{6}u_i$$
$$q_1 = -\frac{1}{6}u_{i-1} + \frac{5}{6}u_i + \frac{1}{3}u_{i+1}$$
$$q_2 = \frac{1}{3}u_i + \frac{5}{6}u_{i+1} - \frac{1}{6}u_{i+2}$$

and

$$\omega_s = \frac{\alpha_s}{\alpha_0 + \cdots + \alpha_{r-1}},$$
$$\alpha_s = \frac{C_s}{\varepsilon + IS_s}, \quad k = 0, \cdots, r-1$$

$$C_0 = 0.1, \quad C_1 = 0.6, \quad C_2 = 0.3$$
$$IS_0 = \frac{13}{12}(u_{i-2} - 2u_{i-1} + u_i)^2 + \frac{1}{4}(u_{i-2} - 4u_{i-1} + 3u_i)^2$$
$$IS_1 = \frac{13}{12}(u_{i-1} - 2u_i + u_{i+1})^2 + \frac{1}{4}(u_{i-1} - 4u_i + 3u_{i+1})^2$$
$$IS_2 = \frac{13}{12}(u_i - 2u_{i+1} + u_{i+2})^2 + \frac{1}{4}(u_i - 4u_{i+1} + 3u_{i+2})^2$$

where, $\varepsilon = 10^{-6}$ is introduced to avoid the denominator becoming zero.

The u^R is reconstructed following the symmetry rule as that to the u^L at interface $i + 1/2$.

In this paper, the WENO scheme described above is used to evaluate the conservative variables with 5th order accuracy. The interface flux is then approximated with 5th order accuracy based on the approximate Riemann solver of the Roe scheme and the LED scheme based on:

$$E_{i+\frac{1}{2}} = E(Q^L_{i+\frac{1}{2}}, Q^R_{i+\frac{1}{2}}) \tag{37}$$

2.6 The Time discretization

For the one-dimensional shock tube problems in this paper, the high-order Runge-Kutta methods are used for the time integration. The time dependent Euler or Navier-Stokes equations can be written as an ordinary differential equation form:

$$\frac{du}{dt} = L(u),$$

Where, the $L(u)$ stands for all the spatial terms in the governing equations.

The third-order TVD Runge-Kutta scheme [24] can be written as

$$u^{(1)} = u^n + \Delta t L(u^n)$$

$$u^{(2)} = \frac{1}{4}[3u^n + u^{(1)} + \Delta t L(u^{(1)})]$$

$$u^{(n+1)} = \frac{1}{3}[u^n + 2u^{(2)} + 2\Delta t L(u^{(2)})]$$

and the fourth-order Runge-Kutta scheme can be written as

$$u^{(1)} = u^n + \frac{1}{2}\Delta t L(u^n)$$

$$u^{(2)} = u^n + \frac{1}{2}\Delta t L(u^{(1)})$$

$$u^{(3)} = u^n + \Delta t L(u^{(2)})$$

$$u^{(n+1)} = \frac{1}{3}[-u^n + u^{(2)} + 2u^{(2)} + u^{(3)}] + \frac{1}{6}\Delta t L(u^{(3)})]$$

For multi-dimensional steady state problems, the implicit time marching scheme is used with the unfactored Gauss-Seidel line relaxation.

3 Results and Discussion

According to Godunov[25], when there are discontinuities in the solutions, monotone behavior of a solution can not be assured with higher than first order scheme. Hence, for an upwind scheme to be used as a Riemann solver, it is essential to examine the performance of the scheme using first order accuracy. For the following test cases, both the 1st order scheme and the 5th WENO scheme are used.

For all the 2D flows calculated in this paper, the strategy of using increased value of $\varepsilon = 10^{-2}$ to minimize the numerical dissipation and to improve convergence [26] is employed.

3.1 Shock Tubes

3.1.1 The Sod Problem

The Sod shock tube problem has the initial solution set to be at rest with a diaphragm located in the the middle of the shock tube. The pressure on the left side of the diaphragm is 10 times higher than the pressure on the right side. At time level t=0, the diaphragm breaks. A shock wave propagates to the right side of the tube. A contact surface follows the shock tube traveling toward the right side at a lower speed. An expansion wave propagates to the left side of the tube. Since the computation stops before the waves

reach either end of the shock tube, the first order extrapolation boundary conditions are used at both ends of the shock tube.

Fig. 1 is the first order accuracy results of the Sod shock tube[27] temperature profiles computed by the present scheme, Roe scheme and the analytical results. The maximum CFL numbers without generating oscillations for this shock tube computation is 1.0 for the present scheme and 0.95 for the Roe scheme. Fig. 1 shows that the present scheme captures the shock profile using 3 grid points while the Roe scheme uses 4 grid points. The contact surface profiles resolved by both the schemes with 1st order accuracy are severely smeared are virtually the same.

Fig. 2 and 3 are the Sod shock tube results calculated with 5th order WENO scheme and 4th order Runge-Kutta method. Obviously, the overall profiles are much more accurate than the 1st order scheme. The expansion front and tail are accurately resolved and the contact discontinuity is sharply captured. The shock profile is about the same as the 1st order result and is primarily determined by the Riemann solver.

Fig. 4 is the temperature profiles calculated by the 5th order WENO and the present E-CUSP scheme at two different CFL numbers varied by 10 times. Fig. 4 indicates that the two profiles are basically identical, which means that the 5th order WENO scheme with 4th order Runge-Kutta method preserves the time accuracy well and the solutions are insensitive to the time steps.

3.1.2 Slowly Moving Contact Surface

This is a shock tube case used in [5] to demonstrate the capability of the scheme to capture the contact surface. The initial conditions are $[\rho, u, p]_L = [0.125, 0.112, 1.0]$, $[\rho, u, p]_R = [10.0, 0.112, 1.0]$. All the results are first order accuracy. Fig. 5 shows that both the present scheme and the Roe scheme can resolve the exact contact surface as they are designed. The results of those schemes are at time level 0.01. The velocity is uniformly constant and the density discontinuity is monotone. The new E-CUSP scheme has far higher CFL number than the Roe schemes with the CFL value of 1.0. The Roe scheme has the maximum CFL=0.3 without generating oscillations. Fig. 5 indicates that as a Riemann solver, both the present scheme and the Roe scheme can capture the exact contact discontinuity. Unfortunately, for the 5th order WENO scheme with the 4th order Runge-Kutta method, it can not achieve the constant velocity and pressure across the contact discontinuity with no oscillation for both the new E-CUSP and Roe scheme. The reason is unknown and is being investigated.

3.1.3 Shock Interaction with an Entropy Wave

This test case is taken from Ref.[28], which represents a Mach 3 shock wave interacting with a sine entropy wave. The initial condition is

$$(\rho, u, p) = \begin{cases} (3.857143, 2.629369, 10.3333), & x < -4, \\ (1 + \varepsilon sin(5x), 0, 1), & x \geq -4 \end{cases}$$

Fig. 6 is the density distribution calculated by the new scheme and the Roe scheme with the 5th-WENO scheme and the 4th order Runge-Kutta method based on the mesh size of 400 points. Both schemes achieve virtually the same profile. Compared with the accurate solutions calculated using 8000 mesh points, the shock profile and the front of the entropy wave are resolved well, but some of the wave amplitudes are under-predicted due to the numerical dissipation.

3.2 Entropy condition

This case is to test if a scheme violates the entropy condition by allowing expansion shocks. The test case is a simple quasi-1D converging-diverging transonic nozzle[16, 17]. The correct solution should be a smooth flow from subsonic to supersonic with no shock. However, for an upwind scheme which does not satisfy the entropy condition, an expansion shock may be produced.

For the subsonic boundary conditions at the entrance, the velocity is extrapolated from the inner domain and the other variables are determined by the total temperature and total pressure. For supersonic exit boundary conditions, all the variables are extrapolated from inside of the nozzle. The analytical solution was used as the initial flow field. Explicit Euler time marching scheme was used to seek the steady state solutions. All the schemes use first order differencing.

Fig. 7 is the comparison of the analytical and computed Mach number distributions with 201 mesh points using the present scheme and the Roe scheme. The analytical solution is smooth throughout the nozzle and reaches the sonic speed at the throat (the minimum area of the nozzle, located at $X/h = 4.22$). It is seen that the Roe scheme generate a strong expansion shock at the nozzle throat. Both schemes can converge to machine zero (12 order of magnitude) with CFL=0.95 even with the expansion shock waves. Similar to the original Zha CUSP scheme[18], the present scheme does not have an expansion shock wave at the sonic point, but is not smooth and has a little glitch. As reported in [16], when the mesh is refined, the amplitude of the expansion shock waves is reduced. When the 2nd order scheme is used, the expansion shock waves disappear.

3.3 Supersonic Laminar Wall Boundary Layer

To examine the numerical dissipation of the new scheme, a laminar supersonic boundary layer on an adiabatic flat plate is calculated using first order accuracy. The incoming Mach number is 2.0. The Reynolds number based on the length of the flat plate is 40000. The Prandtl number of 1.0 is used in order to compare the numerical solutions with the analytical solution. The baseline mesh size is 41×31 in the direction along the plate and normal to the plate respectively. The height of the computational domain is 0.82 times of the flat plate length. There are 13 points within the boundary layer.

Fig.8 is the comparison between the computed velocity profiles and the Blasius solution. The solutions of the present scheme and the Roe scheme all agree precisely with the analytical solution.

Fig.9 is the comparison between the computed temperature profiles and the Blasius solution. Again, the present scheme and Roe scheme accurately predict the temperature profiles and the computed solutions basically go through the analytical solution.

The 1st order accuracy results presented here indicate that the present E-CUSP scheme has low diffusion as the Roe scheme. For the upwind schemes with high diffusion such as the Van Leer scheme, they can not resolve the boundary layer profiles accurately[18, 20].

Fig.10 and 11 are the comparison between the computed velocity and temperature profiles using the WENO scheme and the Blasius solution. Again, they agree very well as expected. The L2-Norm residual can be driven to machine zero.

3.4 Subsonic Flat Plate Turbulent Boundary Layer

The subsonic flat plate turbulent boundary layer is used as the second 2-D test example. In this case, the Baldwin-Lomax turbulence model is used. The computation domain is taken to be $[0, 1] \times [0, 1]$. The cell size is 180×80. The non-dimensional distance y^+ of the first point to the wall is kept under 0.2. The inlet

Mach number is 0.5, and the Reynolds number is 4×10^6 based on the plate length. The flow is subsonic at inlet and outlet.

Fig. 12 is the velocity profile of the subsonic turbulent boundary layer using 5th order WENO scheme. Both the Roe scheme and the present LDE scheme give virtually identical results.

3.5 Transonic Converging-Diverging Nozzle

To examine the performance of the new scheme with 5th order WENO scheme in two-dimensional flow and the capability to capture the shock waves which do not align with the mesh lines, a transonic converging-diverging nozzle is calculated as inviscid flow. The nozzle was designed and tested at NASA and was named as Nozzle A1[29]. The solution is steady state and the time marching is achieved by the unfactored implicit Gauss-Seidel iteration. The nozzle is symmetric about the centerline. Hence only upper half of the nozzle is calculated. The upper boundary uses the slip wall boundary conditions and the lower boundary of the center line uses the symmetric boundary conditions. The mesh size is 175×50. The grid is clustered near the wall. The inlet Mach number is 0.22. The CFL number of 10 is used.

Fig. 13 is the computed pressure contours showing the oblique shock and its reflection on the wall. It is worth pointing out that the shock is so weak that it is not resolved and visible in the pressure contours when the 3rd order MUSCL scheme with the same grid is used. Fig. 14 is the computed nozzle surface pressure coefficient using the 5th order WENO schemes with the LDE scheme and the Roe scheme, which shows that the results computed by the two schemes are indistinguishable.

3.6 Transonic RAE2822 Airfoil

To further examine the LDE scheme with 5th order WENO scheme for transonic flows, the steady state solution of the transonic RAE2822 airfoil is calculated using the Reynolds averaged Navier-Stokes equations with the Baldwin-Lomax turbulence model. The mesh size is 128×55, the freestream Mach number M_∞ is 0.729, the Reynolds number based on chord is 6.5×10^6, and the angle of attack is 2.31^o.

Fig. 15 is the comparison of the computed pressure coefficients using the WENO schemes with experiment, which shows that the results computed by both the LDE and the Roe scheme are in good agreement with the experiment. The pressure contours given in Fig. 16 shows the shock wave captured on the suction surface and indicates that the overall flow field is smooth.

4 Conclusions

The low diffusion E-CUSP scheme presented in this paper appears to be robust to be used with 5th order WENO scheme. The LDE scheme has low diffusion and is able to resolve wall boundary layer accurately and capture crisp shock profiles and exact contact surfaces. For a 1D transonic nozzle, the Roe scheme generates an expansion shock wave at the the sonic point, whereas the LDE scheme proposed in this paper does not. Several 1D shock tube flows and 2D transonic flows are calculated using the 5th order WENO scheme with the LDE scheme. The results of the LDE scheme are in good agreement with experiment, theoretical results, and the results of the Roe scheme.

5 Acknowledgment

This work is partially supported by AFOSR Grant F49620-03-1-0253 monitored by Dr. Fariba Fahroo, by ARO grant 56827-RT-ISP monitored by Lt Col. R. Jefferies at AFOSR and J. Haire at ARO, and by *Miami Wind*^{TR} at University of Miami.

References

[1] X.D.Liu, S.Osher, and T.Chan, "Weighted essentially non-oscillatory schemes," *J.Comput.Phys.*, vol. 126, pp. 200–212, 1994.

[2] G.S. Jiang, and C.W. Shu, "Efficient implementation of weighted ENO schemes," *J.Comput.Phys.*, vol. 126, pp. 202–228, 1996.

[3] P. Roe, "Approximate Riemann Solvers, Parameter Vectors, and Difference Schemes," *Journal of Computational Physics*, vol. 43, pp. 357–372, 1981.

[4] M.-S. Liou and C. J. Steffen, "A New Flux Splitting Scheme," *Journal of Computational Physics*, vol. 107, pp. 1–23, 1993.

[5] Y. Wada and M.-S. Liou, "An Accurate and Robust Splitting Scheme for Shock and Contact Discontinuities." AIAA Paper 94-0083, 1994.

[6] M.-S. Liou, "Progress Towards an Improved CFD Methods: AUSM$^+$." AIAA Paper 95-1701-CP, June, 1995.

[7] M.-S. Liou, "A Sequel to AUSM: AUSM$^+$," *Journal of Computational Physics*, vol. 129, pp. 364–382, 1996.

[8] M.-S. Liou, "Ten Years in the Making-AUSM-Family." AIAA 2001-2521, 2001.

[9] D. Hänel, R. Schwane, and G. Seider, "On the Accuracy of Upwind Schemes for the Solution of the Navier-Stokes Eqautions." AIAA paper 87-1105 CP, 1987.

[10] J. R. Edwards, "A Low-Diffusion Flux-Splitting Scheme for Navier-Stokes Calculations." AIAA Paper 95-1703-CP, June, 1995.

[11] J. R. Edwards, "A Low-Diffusion Flux-Splitting Scheme for Navier-Stokes Calculations," *Computer & Fluids*, vol. 6, pp. 635–659, 1997.

[12] A. Jameson, "Analysis and Design of Numerical Schemes for Gas Dynamics I: Artificial Diffusion, Upwind Biasing, Limiters and Their Effect on Accuracy and Multigrid Convergence in Transonic and Hypersonic Flow." AIAA Paper 93-3359, July, 1993.

[13] A. Jameson, "Analysis and Design of Numerical Schemes for Gas Dynamics I: Artificial Diffusion, Upwind Biasing, Limiters and Their Effect on Accuracy and Multigrid Convergence in Transonic and Hypersonic Flow," *Journal of Computational Fluid Dynamics*, vol. 4, pp. 171–218, 1995.

[14] A. Jameson, "Analysis and Design of Numerical Schemes for Gas Dynamics II: Artificial Diffusion and Discrete Shock Structure," *Journal of Computational Fluid Dynamics*, vol. 5, pp. 1–38, 1995.

[15] G.-C. Zha and E. Bilgen, "Numerical Solutions of Euler Equations by Using a New Flux Vector Splitting Scheme ," *International Journal for Numerical Methods in Fluids*, vol. 17, pp. 115–144, 1993.

[16] G.-C. Zha, "Numerical Tests of Upwind Scheme Performance for Entropy Condition ," *AIAA Journal*, vol. 37, pp. 1005–1007, 1999.

[17] G.-C. Zha, "Comparative Study of Upwind Scheme Performance for Entropy Condition and Discontinuities." AIAA Paper 99-CP-3348, June 28- July 1, 1999.

[18] G.-C. Zha and Z.-J. Hu, "Calculation of Transonic Internal Flows Using an Efficient High Resolution Upwind Scheme," *AIAA Journal*, vol. 42, No. 2, pp. 205–214, 2004.

[19] G.-C. Zha, "Low Diffusion Efficient Upwind Scheme ," *AIAA Journal*, vol. 43, 2005.

[20] G.-C. Zha, "A Low Diffusion E-CUSP Upwind Scheme for Transonic Flows." AIAA Paper 2004-2707, to appear in AIAA Journal, 34th AIAA Fluid Dynamics Conference, June 28 - July 1 2004.

[21] B. Van Leer, "Flux-Vvector Splitting for the Euler Equations," *Lecture Note in Physics*, vol. 170, pp. 507–512, 1982.

[22] B. Baldwin and H. Lomax, "Thin Layer Approximation and Algebraic Model for Separated Turbulent Flows." AIAA Paper 78-257, 1978.

[23] G.-C. Zha, Y. Shen, and B. Wang, "Calculation of Transonic Flows Using WENO Method with a Low Diffusion E-CUSP Upwind Scheme." AIAA Paper 2008-0745, 46th AIAA Aerospace Sciences Meeting, Reno, NV, Jan. 2008.

[24] C.-W. Shu, "Essentially Non-Oscillatory and Weighted Essentially Schemesfor Hyperbolic Conservation Laws." NASA/CR-97-206253, 1997.

[25] S. Godunov, "Finite-Difference Method for Numerical Computation of Discontinuous Solutions of the Equations of Fluid Dynamics," *Mat. Sb.*, vol. 47, pp. 271–306, 1959.

[26] Y.-Q. Shen, B.-Y. Wang, and G.-C. Zha, "Implicit WENO Scheme and High Order Viscous Formulas for Compressible Flows ." AIAA Paper 2007-4431, 2007.

[27] G. Sod, "A survey of several finite difference methods for systems of nonlinear hyperbolic conversation laws," *Journal of Computational Physics*, vol. 27, pp. 1–31, 1978.

[28] C.-W. Shu and O. Osher, "Efficient Implementation of Essentially Non-Oscillatory Shock Capturing Schemes," *Journal of Computational Physics*, vol. 77, pp. 439–471, 1988.

[29] M. L. Mason and L. E. Putnam, "The Effect of Throat Contouring on Two-Dimensional Converging-Diverging Nozzles at Static Conditions ." NASA Technical Paper 1704, 1980.

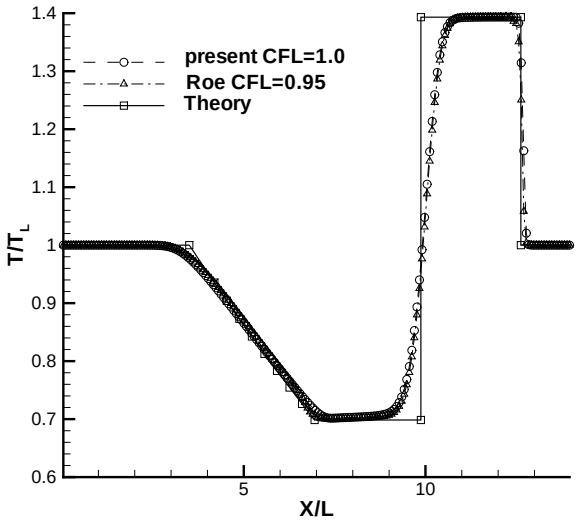

Figure 1: Computed temperature distributions of the Sod 1D shock tube using 1st order schemes.

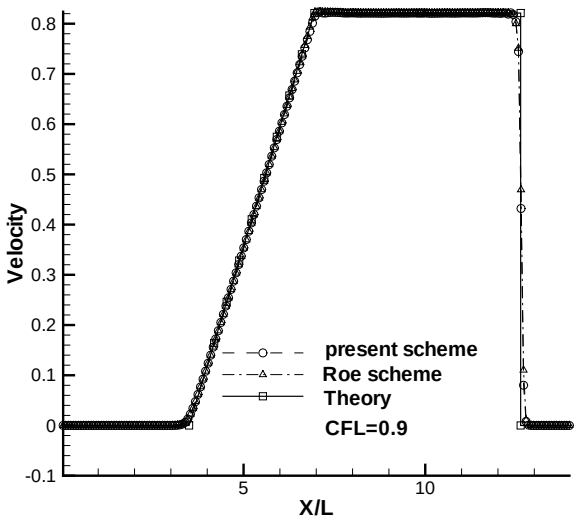

Figure 3: Computed velocity profile of the Sod 1D shock tube using 5th order WENO schemes.

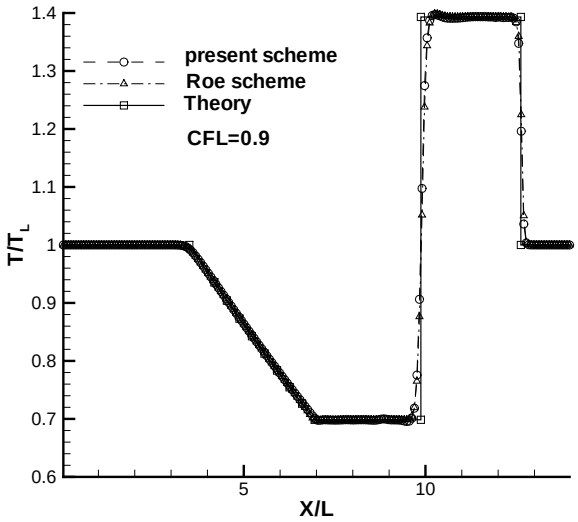

Figure 2: Computed temperature distributions of the Sod 1D shock tube using 5th order WENO schemes.

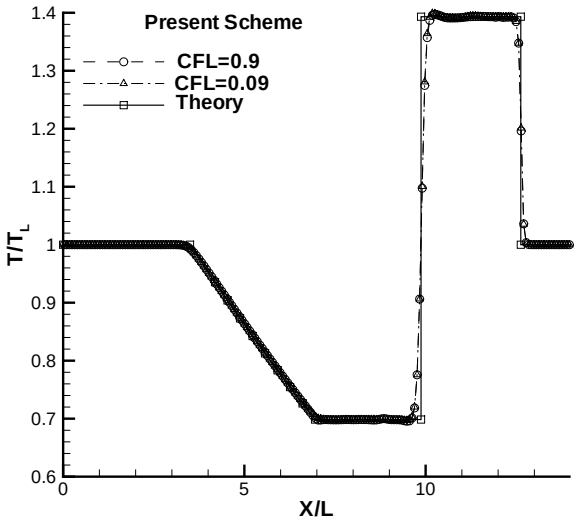

Figure 4: Computed temperature distributions of the Sod 1D shock tube using 5th order WENO schemes with different time steps.

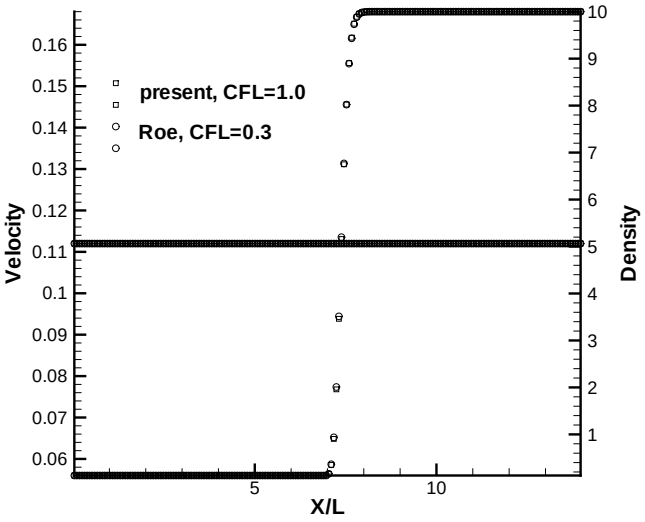

Figure 5: Computed density and velocity profiles of the slowly moving contact discontinuity using 5th order WENO schemes

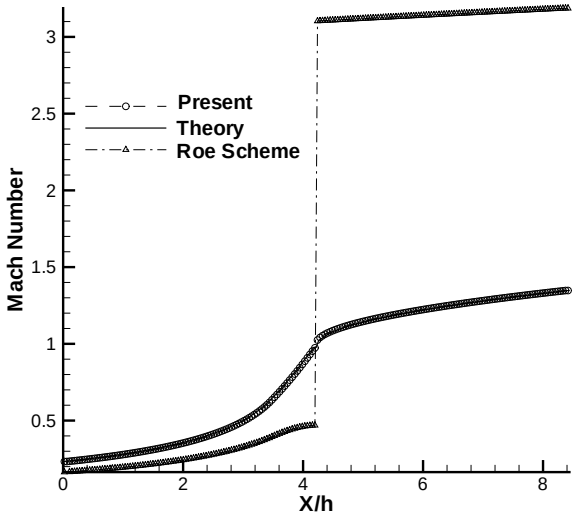

Figure 7: Computed Mach number distributions for the quasi-1D converging-diverging nozzle using 1st order schemes

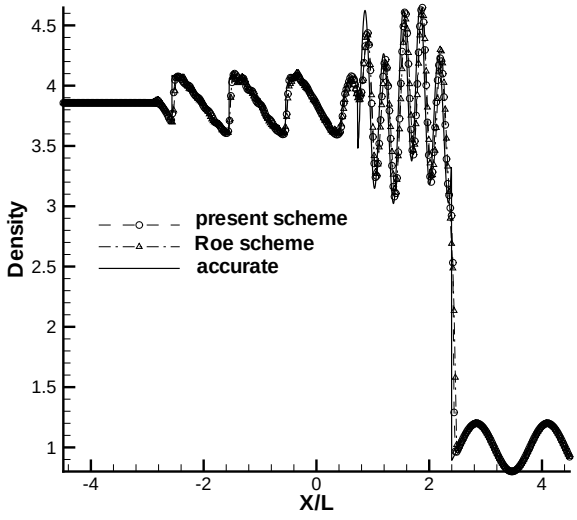

Figure 6: Computed density profiles of the shock interaction with an entropy wave using 5th order WENO schemes

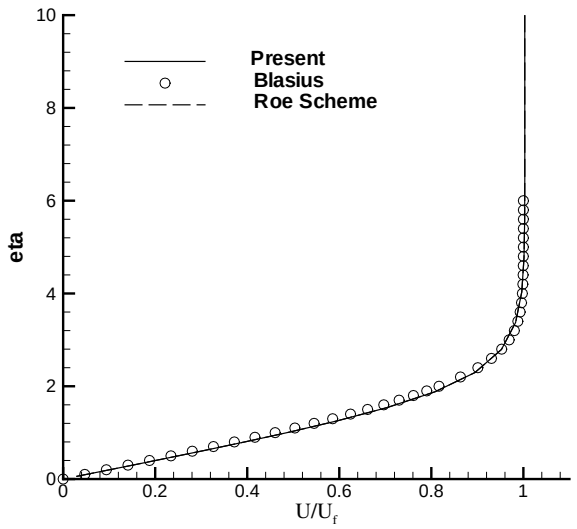

Figure 8: Computed velocity profiles of the laminar boundary layer using 1st order schemes

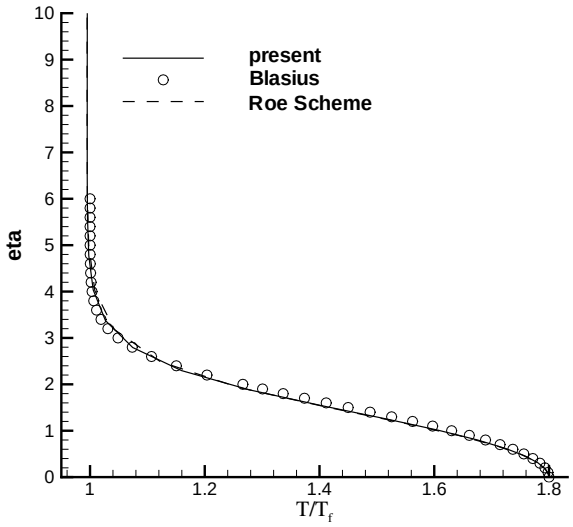

Figure 9: Computed temperature profiles of the laminar boundary layer using 1st order schemes

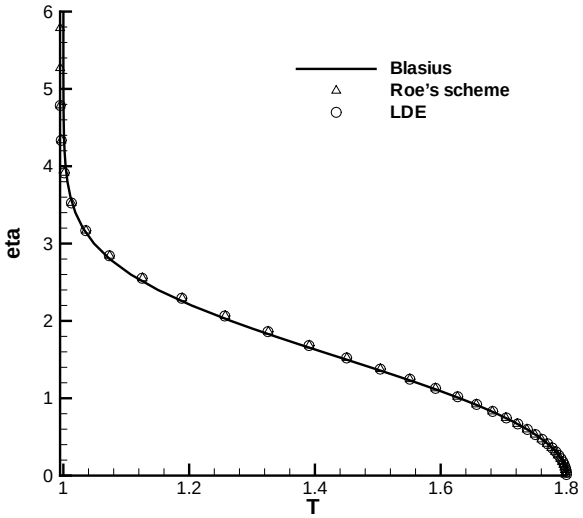

Figure 11: Computed temperature profiles of the laminar boundary layer using 5th order WENO schemes.

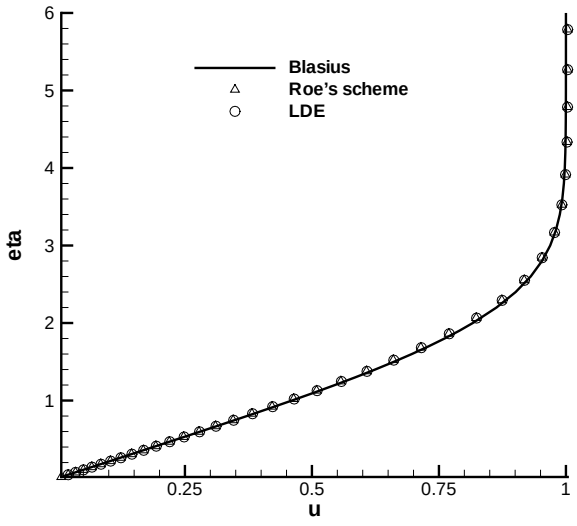

Figure 10: Computed velocity profiles of the laminar boundary layer using 5th order WENO schemes.

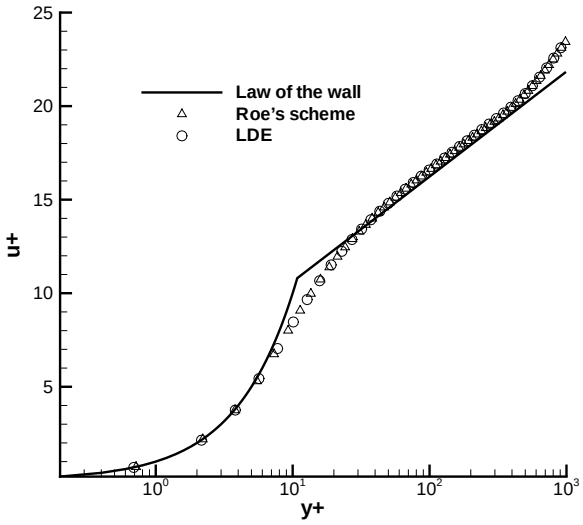

Figure 12: Computed velocity profile of the subsonic turbulent boundary layer using 5th order WENO schemes

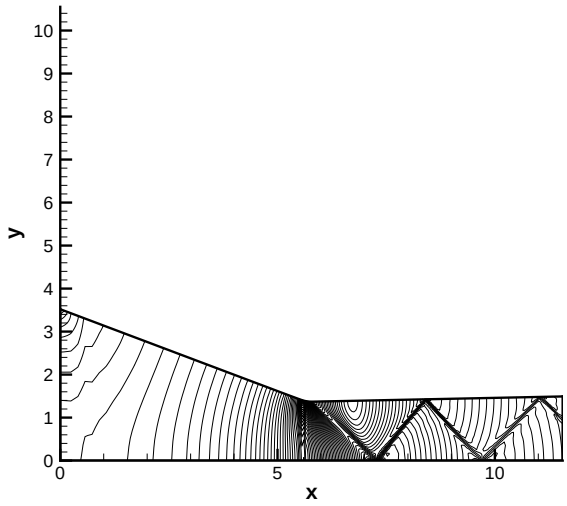

Figure 13: Computed nozzle pressure contours using the 5th WENO and the new E-CUSP scheme

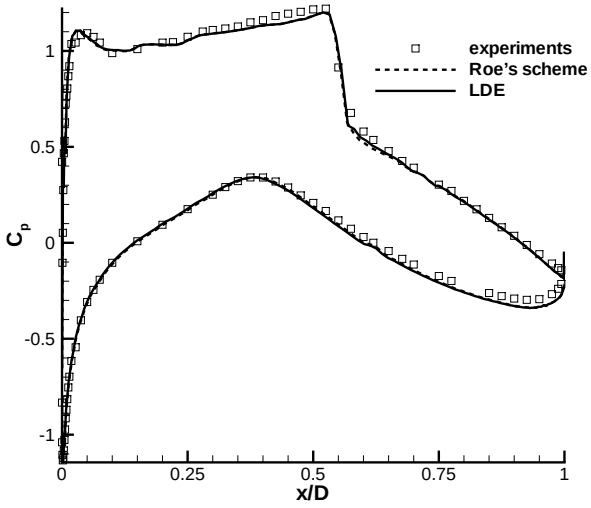

Figure 15: Computed RAE2822 airfoil surface pressure coefficient using the 5th order WENO schemes

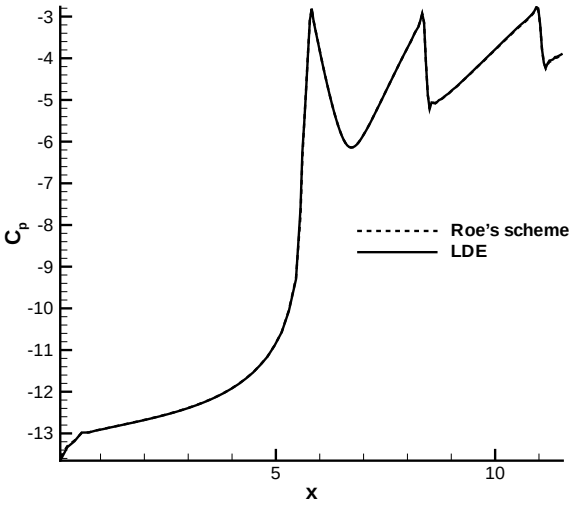

Figure 14: Computed nozzle surface pressure coefficient using the 5th order WENO schemes

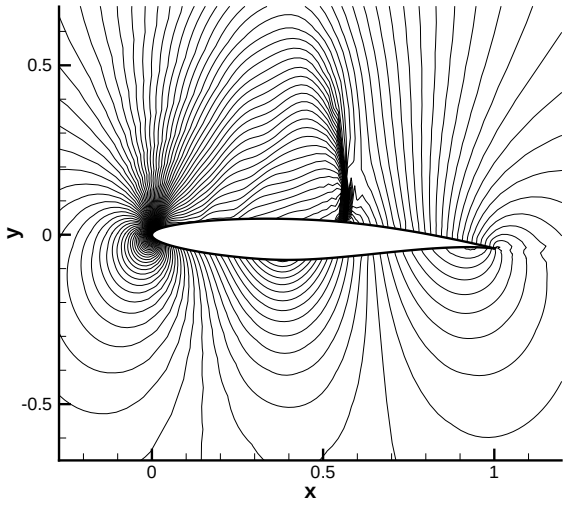

Figure 16: Computed RAE2822 airfoil pressure contours using the 5th WENO and the new E-CUSP scheme